21th Annual Workshop on
Mathematical Problems in Industry
Worcester Polytechnic Institute, June 13–17, 2005

Analysis of Chemical-Mechanical Polishing via Elastohydrodynamic Lubrication

Problem presented by
Len Borucki
Araca Incorporated/Intelligent Planar
Tucson Arizona 85750

	A. Bhattacharya	C. Breward	M. Gratton
Participants:	J. Evans	M. Nicholas	C. Please
	D. Schwendeman	M. Surles	T. Witelski

Summary Presentation given by M. Gratton and J. Evans (6/17/05)
Summary Report prepared by T. Witelski and C. Breward
(May 22, 2006 version)

1 Introduction

Chemical-Mechanical Polishing (CMP) is an essential process in the manufacturing of microprocessors on silicon wafers. To reliably deposit a complicated layer of integrated circuits, the surface of the substrate material must be carefully prepared so that it is sufficiently smooth and level; this process is called planarization. CMP accomplishes this through a combination of mechanical and chemical means: a polishing pad made of a soft polymeric material is rubbed against the surface of the silicon wafer, see schematics in Fig. 1(left). Related to the porous structure of the pad material, the pad's surface is very rough and irregular and is generally characterized in an statistical manner in terms of the distribution of local micro-scale peaks, called asperities, on the surface, see Fig. 1(right). When pressed against the wafer by an applied load, the pad asperities will flatten at positions where they come in contact with the wafer. See Fig. 2 for a schematic representation of the asperities and the wafer surface; for convenience we will consider an inverted configuration with the pad above the wafer.[1] The applied load and the density of asperities will determine the actual area in microscopic contact between the wafer and the pad. Acting alone, the pad will primarily act to sweep away debris from the wafer surface.

An additional key component in effective CMP processes is a liquid slurry containing fine abrasive particles. The slurry fluid covers the wafer surface and can contain moderate to high concentrations of abrasive particles. The fluid will prevent the asperities from coming in direct contact with the wafer ("dry contact"). Instead, there will be a thin layer of fluid passing between the asperity and the wafer; the dynamics of this fluid layer can be described by low Reynolds number lubrication theory [2, 9]. We will make use of elastohydrodynamic lubrication theory (EHL) to describe the interaction between the slurry fluid and the deformation of the asperities. In particular we will determine the thickness of this layer in terms of the load and other system

[1] In our analysis the influence of gravity will be negligible, so the vertical orientation of the pad and wafer does not affect our results.

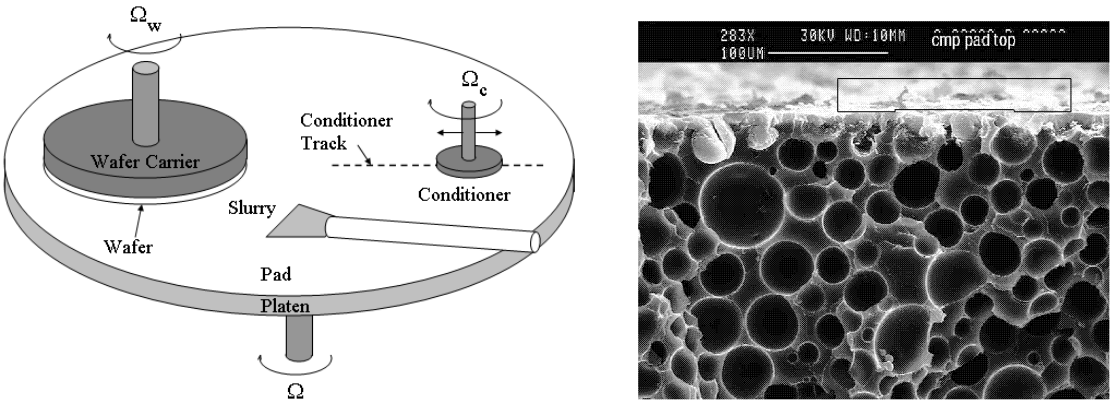

Figure 1: (Left) Schematic of a typical single-wafer rotary CMP tool. (Right) Scanning Electron Micrograph cross-section of a used, conditioned void-filled polyurethane polishing pad. Surface asperities can be seen in the boxed region at the top of the image. The scale bar at the top center is 100 microns (0.1 mm) long. Voids average about 30 microns in diameter and occupy about 60% of a planar cross-section (Data by Letitia Malina, Motorola).

parameters. This in turn will allow us to estimate a coefficient of friction and a rate of heat generation due to the polishing.

The action of the abrasive particles in the slurry is crucial to smoothing the wafer surface. It is understood that particles that become trapped in the EHL layers of asperities will be pressed into the wafer surface with sufficient force to remove material and to yield planarization effects. The abrasive action of the particles is partially due to temperature-dependent chemical effects. While many questions regarding the dynamics of the slurry particles and their possible influence on the EHL solution remain open, we will comment on the range of particle sizes that may dominate the CMP process.

In section 2, we review results on dry contact from classical solid mechanics [15]. In section 3, we describe the elasto-hydrodynamic lubrication analysis of the fluid flow (no particles) in the gap under a deformed asperity. In section 4, we calculate the corresponding rise in temperature due to

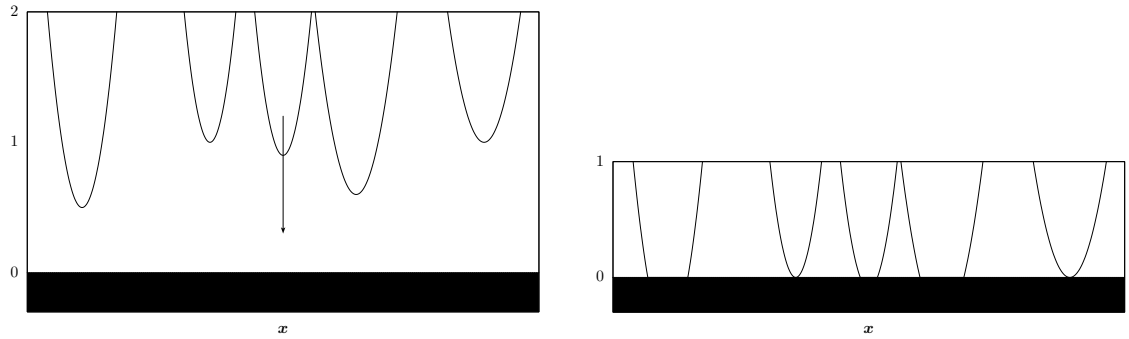

Figure 2: Schematic representations of the the wafer surface (solid black), $z = 0$, and the asperities on the pad surface (upper surface): (left) being brought into contact, (right) in contact, with some asperity tips being deformed.

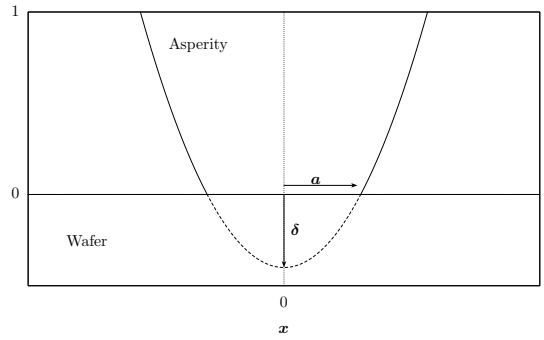

Figure 3: Schematic representation of a deformed asperity in idealized dry contact with the wafer surface.

the heat generated due to the viscous fluid flow. In section 5, we conclude with some remarks on studying the influence of the presence of slurry particles on the preceding models.

2 Dry Contact

The most fundamental problem to be considered in this project is that of direct contact between a single asperity tip and the wafer surface. Describing the deformation of the asperity due to the contact forces and applied load is the classic problem of dry contact between solids [15].

The wafer surface, $z = 0$, is idealized as being flat and rigid. The undeformed asperity is modeled as being locally parabolic at its minimum, with radius of curvature R. The pad material is assumed to be elastic, that is, it deforms in response to locally applied forces. For small applied loads, the deformations are idealized as just squashing the small portion of that asperity tip that would penetrate the wafer surface, see Fig. 3. For a given total normal load n applied to the asperity, the central questions of interest are:

- How far into the wafer will the asperity be pushed?
- What is the contact area of the surfaces in the deformed configuration?

We will consider two simple models of elastic contact in two dimensions[2]: (i) Hertzian contact and (ii) the elastic foundation model. In both cases the forcing and deformation in the asperity are assumed to be restricted to the contact area and the deformed asperity height profile is given by (see Fig. 3)

$$z(x) = \begin{cases} -\delta + \frac{1}{2R}x^2 & |x| \geq a, \\ 0 & |x| \leq a. \end{cases} \tag{1}$$

This model is a reasonable approximation for small deformation (δ small) and idealizes the pad material as being perfectly compressible given sufficient applied force. From (1) it follows that the tip deformation is related to the radius of the contact area by

$$\delta = \frac{a^2}{2R}. \tag{2}$$

[2]Two-dimensional cross-sections of cylindrical surfaces, $z = f(x)$. Analogous results are also known for axisymmetric contacts, $z = g(r)$.

Equivalently, this allows us to define a lateral length scale for the contact area in terms of the asperity's radius of curvature and deformation,

$$a = \sqrt{2R\delta}. \tag{3}$$

To complete the model, a relation between the applied load and the deformation or contact area is needed.

A widely used classic model for deformation of linearly-elastic solids in contact is the Hertzian contact model [15]. For two-dimensional cylindrical contacts, solving for the pressure on the contact area, $-a \le x \le a$, yields

$$p(x) = \frac{2n}{\pi a}\sqrt{1 - \frac{x^2}{a^2}}, \tag{4}$$

with $p(x) = 0$ outside the region of contact. Note that the integral of the pressure gives the total applied load in the normal direction, $n = \int_{-a}^{a} p(x)\,dx$.[3] In [15, Chapter 4] it is then shown that the contact radius and tip deformation are given in terms of the load by

$$a = \left(\frac{4R}{\pi E^*}\right)^{1/2}\sqrt{n}, \qquad \delta = \frac{2}{\pi E^*}\,n, \tag{5}$$

where the plane-strain modulus of the pad material, E^*, is given in terms of its Young's modulus and the Poisson ratio,

$$E^* = \frac{E}{1-\nu^2}. \tag{6}$$

For axisymmetric point contacts, with $0 \le r \le a$, the analogous results are

$$a = \left(\frac{3R}{4E^*}\right)^{1/3} n^{1/3}, \qquad \delta = \left(\frac{9}{256E^*R}\right)^{1/3} n^{2/3}. \tag{7}$$

A simpler model of contact deformation that we will also make use of is called the elastic foundation model, or Winkler mattress model [15, Chapter 4]. In this case, spatial coupling between points in the deforming solid is completely neglected and the deformation is described in terms of an array of independent Hooke's law linear springs with spring constant k. That is, the local force density is given by $p(x) = k(\delta - x^2/2R)$. The corresponding pressure takes the form

$$p(x) = \frac{3n}{4a}\left(1 - \frac{x^2}{a^2}\right), \tag{8}$$

where the spring constant can be related to the ratio of applied load to tip deformation by $k = 3n/[4\sqrt{2}R^{1/2}\delta^{3/2}]$. Then the resulting contact area and tip deformation are

$$a = \left(\frac{3R}{2k}\right)^{1/3} n^{1/3}, \qquad \delta = \left(\frac{9}{32k^2R}\right)^{1/3} n^{2/3}. \tag{9}$$

At the most general level, these results qualitatively agree with the Hertzian model: as the applied load increases, so do a and δ. While the numerical coefficients do not match, the scaling dependence on n can be matched between (5) and (9) if the spring constant can be treated as being inversely

[3] $n = 2\pi\int_0^a p(r)r\,dr$ in the axisymmetric problem.

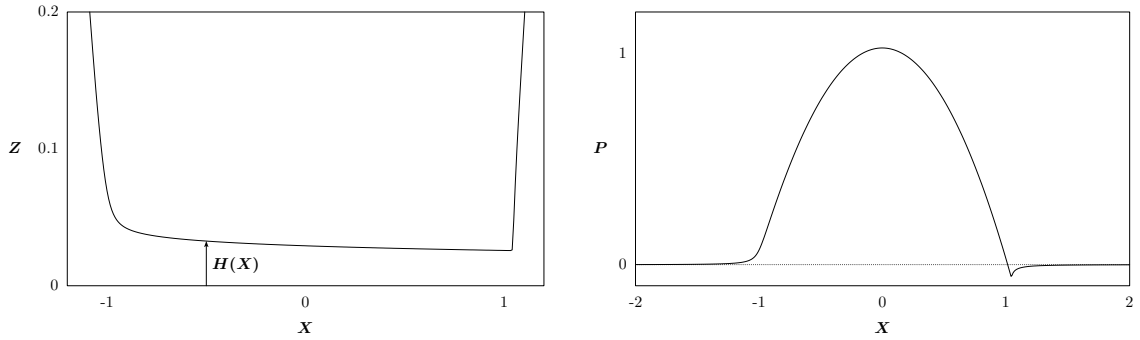

Figure 4: Gap height profile $H(X)$ (left) and nondimensionalized pressure $P(X)$ (right) for $\Lambda = 0.01$ and $B = 0$.

proportional to a [15]. This assumption is somewhat inconsistent with Hooke's law, rather, it describes a nonlinear spring with $p(x) = \tilde{k}\sqrt{\delta - x^2/2R}$, which matches the form of (4).

Once the normal forces (pressures) have been determined, the simplest law for sliding friction involved in polishing is that the tangential force is the normal force times a coefficient of friction, $f = C_f\, n$ [15, Chapter 7].

3 Elastohydrodynamic Lubrication

The next step in our programme to describe the polishing process is to incorporate the influence of a lubricating fluid on the contact dynamics. The presence of the fluid prevents direct contact between the pad and the wafer surface. Instead, forces between the surfaces will be transmitted through the fluid, which is assumed to be viscous and incompressible.

The slow flow of an incompressible viscous fluid through a long, narrow gap can be described by the Reynolds equation [9, 18, 2],

$$\frac{d}{dx}\left(\frac{h^3}{\mu}\frac{dp}{dx}\right) = 6\mathbb{U}\frac{dh}{dx}, \tag{10}$$

where h is the gap height, p is the pressure and μ is the fluid viscosity. This is a low Reynolds number limit of the Navier-Stokes equations in a slender domain [9]. We will use this equation in the reference frame moving with the asperity tip. The wafer is assumed to have a speed $\mathbb{U}$ relative to the asperity tip and generates a shear flow of the fluid in the narrow gap of height $h(x)$ between the deformed tip and the wafer surface, see Fig. 4(left). Equation (10) relates the pressure developed in the fluid to the conditions imposed by the gap geometry, with appropriate boundary conditions. The pressure in the fluid is uniform in the vertical direction over the gap height and gives the normal load per unit area due to both elastic and hydrodynamic effects (EHL).

For simplicity, we make use of the elastic foundation model to describe the deformation of the asperity (8).[4] The hydrodynamic pressure yields additional deformations (taken to be linearly

[4]Similar EHL problems occur in other applications involving deformable roll coating [4, 7]. See [7] for criticism of the use of the elastic foundation model.

proportional to the pressure, $h = p/k$) over those due to the applied forces involved in dry contact.[5] This approximate model has been used in previous studies of CMP [19]. This model has also been called the *constrained column model* (CCM) [7], where it is described that the spring constant can be related to the material properties of the asperity and its total depth D (which can be taken to be on the order of tens of microns),

$$k = \frac{(1-\nu)E}{(1+\nu)(1-2\nu)D}. \tag{11}$$

Consequently, the gap height can be expressed in terms of the pressure as

$$h(x) = \frac{x^2}{2R} - \delta + \frac{p}{k}. \tag{12}$$

We will nondimensionalize quantities relative to the scale of the asperity deformation δ,

$$x = aX \qquad h(x) = \delta H(X) \qquad p(x) = k\delta P(X). \tag{13}$$

Hence we get $H(X) = X^2 - 1 + P(X)$, and the Reynolds equation for the rescaled pressure takes the form

$$\frac{d}{dX}\left([X^2 - 1 + P]^3 \frac{dP}{dX}\right) = \Lambda\left(2X + \frac{dP}{dX}\right) \tag{14}$$

where the dimensionless parameter Λ is the ratio of viscous to elastic effects,

$$\Lambda = \frac{6\mu_0 \mathbb{U} a}{k\delta^3}. \tag{15}$$

Far from the asperity, the fluid pressure will return to the ambient level, described by the asymptotic boundary conditions

$$P(X \to \pm\infty) \to 0, \tag{16}$$

hence P represents the deviation of the pressure from the ambient level. Formally, the pressure contribution to the gap height should only be included only over the range over which dry contact for the asperity tip is expected, $|X| \leq 1$[6]. However, outside this interval, deformations of the pad surface due to the presence of the fluid are also possible and hence the pressure term in $H(X)$ is used on the entire computational domain.[7]

A numerical solution of (14) for small Λ is shown in Fig. 4. The pressure is a small perturbation to the leading order solution expected from the elastic foundation model,

$$P(X) = (1 - X^2) + O(\sqrt{\Lambda}), \qquad \text{for } |X| < 1 \tag{17}$$

with $P(X) \sim \Lambda\tilde{P}(X)$ for $|X| > 1$. The $O(\sqrt{\Lambda})$ contribution to the pressure is asymmetric, determining the gap height, $H = X^2 - 1 + P$, to take the general form of a converging channel, with $dH/dX < 0$ and $H(X) = O(\sqrt{\Lambda})$, see Fig. 4(left).

[5] It might be hoped that a Reynolds equation for EHL based on the Hertzian contact model could be written similarly, with $p = (E^*\delta/a)\sqrt{h}$, but this ad hoc model does not give sensible results. See Szeri [18, section 8.5] for description of an equation giving $h(x)$ in terms of an integral of the pressure.

[6] Sometimes called the negative gap height range

[7] However, in any case, the pressure rapidly approaches zero outside $|X| \leq 1$ and it does not significantly change the solution of (14).

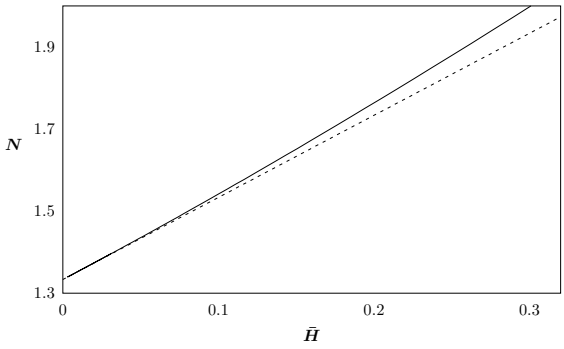

Figure 5: The near-linear relation between average gap height and applied load at fixed δ: solid curve - numerical results, dashed curve - linear behavior for $\bar{H} \to 0$, equation (19).

To gain further understanding of the EHL solution, in Fig. 5 we plot the relation of the mean gap height to the normal load,

$$\bar{H} = \frac{1}{2}\int_{-1}^{1} H(X)\,dX \qquad N = \int_{-\infty}^{\infty} P(X)\,dX, \tag{18}$$

where $n = k\sqrt{2R}\,\delta^{3/2}N$ or $n = O(\Lambda^{-3/5})N$. Note that N is the load in excess of the baseline load needed for dry contact with deformation δ, given by equation (9). Fig. 5 shows that they approximately follow a linear relation,

$$N \sim 2\bar{H} + 4/3 \qquad \bar{H} \to 0, \tag{19}$$

where $N = 4/3$ corresponds to dry contact ($\bar{H} = 0$). This result seems to clash with expectations from classical lubrication theory, where thinner fluid layers correspond to larger pressures and normal loads. In fact there is no conflict as (19) is given with respect to variables nondimensionalized by the asperity tip deformation δ. To achieve a fixed value of δ, a sufficient load must be applied, for dry contact, this is given by (9); (19) can be interpreted as giving the relative change to the equilibrium applied load from EHL effects. In fact, starting from $\bar{H} \sim \frac{1}{3}\sqrt{\Lambda}$ for $\Lambda \to 0$ and using (9) and (15) these results suggest the dimensional scaling relation,

$$\bar{h} \sim \frac{1}{3}\left(\frac{6\mu_0\mathbb{U}\sqrt{2R}}{k}\right)^{1/2}\left(\frac{9}{32k^2R}\right)^{-1/12} n^{-1/6}. \tag{20}$$

This form makes the inverse relationship between the applied load and the film thickness more clear. Results by Grubin [6, 18, 2] and others [18] suggest other possible scalings, but all agree on the direct dependence on the sliding velocity $\mathbb{U}$ and inverse dependence on the load n. There is general agreement that for most practical conditions, EHL introduces relatively small changes to the dry contact pressure [2, 18]. However for CMP these small changes which determine $\bar{h}$ are of central importance.

3.1 Pressure-dependent viscosity

When the pressure varies over a sizable range, it can be important to take into account the dependence of the viscosity on the pressure, this is often assumed to be in an exponential form,

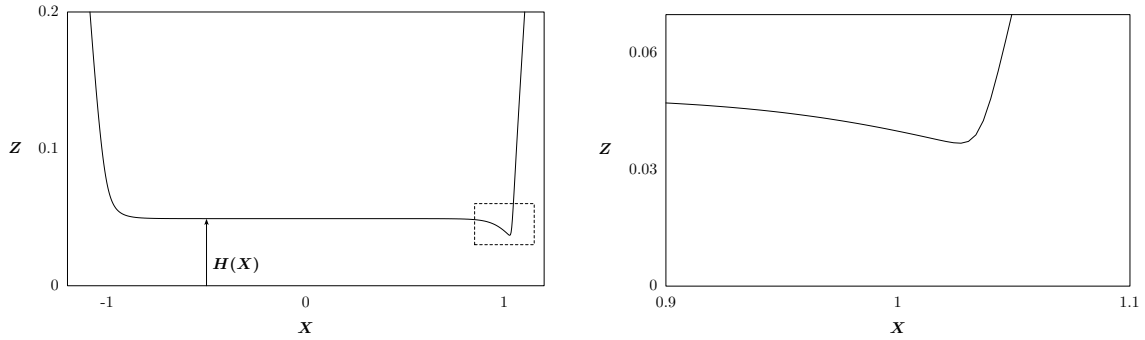

Figure 6: The gap height profile with pressure-dependent viscosity for $\Lambda = 0.01$ and $B = 10$. An enlarged view of the distinctive exit constriction is shown on the right.

$\mu(p) = \mu_0 e^{\beta p}$. The corresponding rescaled Reynolds equation is

$$\frac{d}{dX}\left(\frac{[X^2 - 1 + P]^3}{e^{BP}}\frac{dP}{dX}\right) = \Lambda\left(2X + \frac{dP}{dX}\right) \tag{21}$$

where $B = k\beta\delta$. In regions where the pressure is small, the pressure-dependence has a weak influence, $e^{BP} \sim 1$ for $P \to 0$, and the solution of (21) is well approximated by (14). However, near the center of the asperity ($|X| \ll 1$) where e^{BP} becomes large, we may consider the limit $e^{BP} \to \infty$, in which (21) reduces to $2X + P'(X) = 0$ with solution $P(X) = C + 1 - X^2$ corresponding to $H(X) = C$ (constant to leading order). Indeed, we observe from the numerical results shown in Fig. 6 that the solution yields a nearly constant gap height. There is a noticeable change in $H(X)$ only in a narrow layer at the trailing edge near $X = 1$, called the *exit constriction* [2, section 13.12].[8] This form of solution has been described in previous studies of EHL theory [18, section 8.2]. Even though (21) is a simplified model, it does a good job of capturing most of the qualitative form of the gap height profile. The pressure profile looks very similar to $P(X)$ for $B = 0$ (see Fig. 4(right)); this is notable since many studies suggest the presence of a strong positive pressure spike at the exit constriction [18, 9]. Interestingly, most other features of the solution of (21), like the load-gap relation in Figure 5 is unchanged by the pressure-dependence of the viscosity. We will make use of this solution for our further discussions of thermal effects and slurry particle contributions.

3.2 Viscous drag

Another consequence of our lubrication model for the flow of the slurry between the asperity tip and the wafer is an estimate for the friction due to viscous shear of the fluid. In dimensional form,

[8] Colin Please noted that the exit constriction takes the form of an new miniature asperity on the surface of the flattened asperity. The original asperity itself being a micro-scale structure on a nominally flat surface. This brought to mind the poem on self-similar structures:

> Great fleas have little fleas upon their backs to bite 'em,
> And little fleas have lesser fleas, and so ad infinitum,
> And the great fleas themselves, in turn, have greater fleas to go on,
> While these again have greater still, and greater still, and so on.
> – Augustus de Morgan

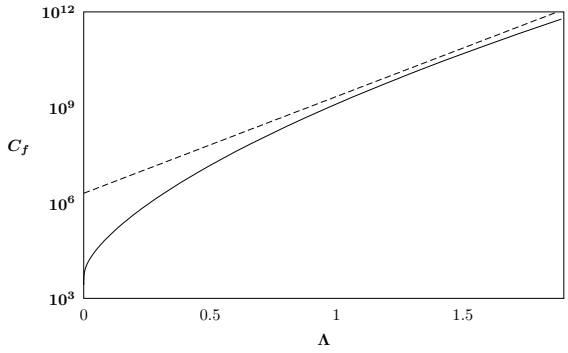

Figure 7: Numerically computed drag coefficient as a function of the speed parameter, $D(\Lambda)$ in the pressure-dependent viscosity case with $B = 10$.

the fluid velocity in the gap is

$$u(z) = -\frac{1}{2\mu(p)}\frac{dp}{dx}(hz - z^2) + \mathbb{U}\left(1 - \frac{z}{h}\right), \qquad 0 \le z \le h. \tag{22}$$

The shear stress at the wafer surface is

$$\mu\frac{\partial u}{\partial z}\bigg|_{z=0} = -\frac{h}{2}\frac{dp}{dx} - \frac{\mu\mathbb{U}}{h}. \tag{23}$$

The total drag force is given by the integral of the shear stress over the contact area,

$$\begin{aligned} \text{drag} &= \int_{-a}^{a} \mu\left|\frac{\partial u}{\partial z}\right| dx = \mathbb{U}\sqrt{2R}\left(\frac{9}{32k^2R}\right)^{-1/6} n^{-1/3} D(\Lambda) \\ &= O(\Lambda^{1/5})D(\Lambda), \end{aligned} \tag{24}$$

where the nondimensional drag function is

$$D(\Lambda) = \int_{-1}^{1} \frac{3H}{\Lambda}\frac{dP}{dX} + \frac{e^{BP}}{H}\, dX. \tag{25}$$

Note that the scaling of the drag in terms of Λ follows from the relations $\Lambda = O(\delta^{-5/2}) = O(n^{-5/3})$. Since H, P depend on Λ, $D(\Lambda)$ is a nontrivial function of Λ. Figure 7 shows a plot of the drag coefficient, $C_f = \text{drag}/n = O(\Lambda^{4/5})D(\Lambda)$. For large B, the drag coefficient grows exponentially with Λ. For smaller B, C_f grows more slowly; for $B = 0$, $C_f = O(\Lambda^{1/4})$.

4 Thermal effects

Having determined a model for the gap height and effective contact area, we now determine the heat generated by viscous dissipation at the asperity tips. The dimensional equation for steady state heat transfer is

$$u\frac{\partial T}{\partial x} + w\frac{\partial T}{\partial z} = \kappa\left(\frac{\partial^2 T}{\partial x^2} + \frac{\partial^2 T}{\partial z^2}\right) + \frac{\mu(p)}{\rho c_p}\left(\frac{\partial u}{\partial z}\right)^2, \tag{26a}$$

on the gap domain, $-a \le x \le a$ and $0 \le z \le h(x)$. Here, κ is the thermal diffusivity, ρ is the density and c_p is the specific heat capacity. We must impose boundary conditions on the wafer and the pad (along with conditions at the inlet and possibly the outlet of the flow). We suppose that the pad is insulating, that is, that there is no flow of heat into the pad. Thus we write

$$\frac{\partial T}{\partial n} = \mathbf{n} \cdot \nabla T = 0, \qquad \text{at} \qquad z = h, \tag{26b}$$

where $\mathbf{n} \propto (-h'(x), 1)$ is the normal to the surface. At the boundary between the liquid and the wafer, we assume continuity of temperature and heat flux, and thus write

$$T = T_w, \qquad D\frac{\partial T}{\partial z} = \frac{\partial T_w}{\partial z}, \qquad \text{at} \qquad z = 0, \tag{26c}$$

where T_w denotes the temperature in the wafer, and D is the ratio of the liquid and solid thermal conductivities. The problem for the temperature in the wafer reads

$$\mathbb{U}\frac{\partial T_w}{\partial x} = \kappa_w \left(\frac{\partial^2 T_w}{\partial x^2} + \frac{\partial^2 T_w}{\partial z^2} \right), \tag{27a}$$

with

$$T_w \to 0 \qquad \text{as} \qquad z \to -\infty, \tag{27b}$$

(along with conditions at the gap inlet and possibly the outlet). We rescale the problem in the liquid layer using

$$x = aX, \qquad z = \delta Z, \quad h = \delta H, \quad u = \mathbb{U}U, \qquad w = (\mathbb{U}\delta/a)W, \qquad T = T_0 + \theta(x,z)\Delta T, \tag{28}$$

where T_0 is an ambient temperature of the liquid upstream of the asperity. The choice of scaling for the temperature rise is consistent with the temperature being uniform in the vertical direction to leading order, with convective and viscous heating effects entering together at next order,

$$\Delta T = \frac{a\mu_0 \mathbb{U}}{\rho c_p \delta^2}. \tag{29}$$

This yields the problem on $0 \le z \le h$

$$\epsilon^2 \mathrm{Pe}\left(U\frac{\partial \theta}{\partial X} + W\frac{\partial \theta}{\partial Z} \right) = \epsilon^2 \frac{\partial^2 \theta}{\partial X^2} + \frac{\partial^2 \theta}{\partial Z^2} + \epsilon^2 \mathrm{Pe}\, e^{BP} \left(\frac{\partial U}{\partial Z} \right)^2, \tag{30a}$$

$$-\epsilon^2 \frac{dH}{dX}\frac{\partial \theta}{\partial X} + \frac{\partial \theta}{\partial Z} = 0, \qquad \text{on } Z = H, \tag{30b}$$

$$\frac{D\epsilon_w}{\epsilon}\frac{\partial \theta}{\partial Z} = \frac{\partial \theta_w}{\partial \zeta}, \qquad \theta = \theta_w \qquad \text{on } Z = 0. \tag{30c}$$

The problem in the wafer, $z \le 0$, follows similarly with the scalings,

$$z = \zeta\sqrt{a\kappa_w/U}, \qquad T_w = T_0 + \theta_w(X,\zeta)\Delta T, \tag{31}$$

$$\frac{\partial \theta_w}{\partial X} = \epsilon_w^2 \frac{\partial^2 \theta_w}{\partial X^2} + \frac{\partial^2 \theta_w}{\partial \zeta^2}, \tag{32a}$$

$$\frac{D\epsilon_w}{\epsilon}\frac{\partial\theta}{\partial Z} = \frac{\partial\theta_w}{\partial\zeta}, \quad \theta = \theta_w \qquad \text{on } \zeta = 0, \tag{32b}$$

$$\theta_w \to 0 \qquad \text{as } \zeta \to -\infty. \tag{32c}$$

The parameters in these equations are

$$\epsilon = \frac{\delta}{a}, \qquad \epsilon_w = \frac{1}{\sqrt{\mathrm{Pe}_w}}, \qquad \mathrm{Pe} = \frac{\mathbb{U}a}{\kappa}, \qquad \mathrm{Pe}_w = \frac{\mathbb{U}a}{\kappa_w}, \tag{33}$$

and the two problems are coupled through the boundary conditions at $z = 0$, equations (30c) and (32b).

4.1 Solution in the slurry when boundaries are both insulating

First, we suppose that $1/(D\epsilon\epsilon_w) \ll 1$, this can be shown to imply that contributions to the vertical heat flux out of the gap in (30c) enter only at higher order. This is the worst case scenario, when the none of the heat generated in the lubrication gap diffuses into the wafer or the polishing pad materials. Assuming that $\mathrm{Pe} \sim O(1)$, the temperature is uniform across the thickness of the layer, and we must proceed to next order in the lubrication theory expansion of the problem for $\epsilon \to 0$ to determine the equation for the leading-order temperature [11, 14]. We find that

$$\mathrm{Pe}H\bar{U}\frac{d\theta}{dX} = \frac{d}{dX}\left(H\frac{d\theta}{dX}\right) + \mathrm{Pe}\, e^{BP}\int_0^H \left(\frac{\partial U}{\partial Z}\right)^2 dZ \tag{34a}$$

where the depth-averaged velocity is

$$\bar{U}(X) \equiv \frac{1}{H(X)}\int_0^{H(X)} U(X,Z)\, dZ = \frac{1}{2} - \frac{1}{2\Lambda e^{BP}}H^2\frac{dP}{dX}, \tag{34b}$$

and the heat generated due to viscosity is

$$e^{BP}\int_0^H (\partial_Z U)^2\, dZ = \frac{e^{BP}}{H} + \frac{3H^3}{\Lambda^2 e^{BP}}\left(\frac{dP}{dX}\right)^2. \tag{34c}$$

We solve (34a) subject to the boundary conditions that upstream of the asperity tip the temperature is at the ambient level,

$$\theta \to 0 \qquad \text{as} \qquad X \to -\infty, \tag{34d}$$

and downstream, that none of the heat generated in the gap is dissipated,

$$\frac{\partial\theta}{\partial X} \to 0 \qquad \text{as} \qquad X \to \infty. \tag{34e}$$

We show results from numerical solution of this problem in Figure 8. In general, the results follow expectations: the temperature profiles are monotone increasing along the gap and increasing the viscosity (through B) at fixed Λ yields a large rise in temperature. It is interesting to observe that while for $B = 0$, the temperature rise scales as $\theta_{\max} = O(\Lambda^{-1})$, for $B > 0$ the $\theta_{\max}(\Lambda)$ has a minimum at a finite value of Λ. This can be plausibly due to the competition between the two terms in (34c).

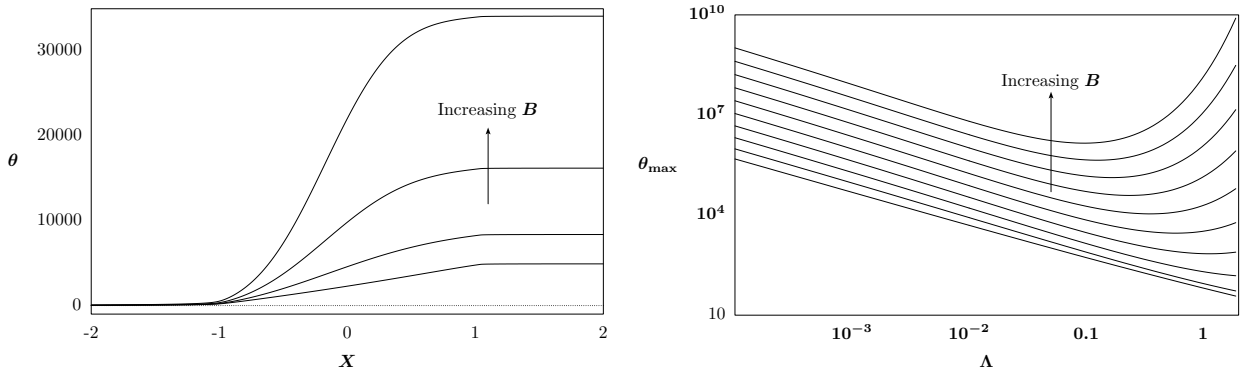

Figure 8: (left) Scaled temperature profiles for $\Lambda = 0.01$, Pe $= 10$ and $B = 0, 1, 2, 3$. (right) Maximum scaled temperature as a function of Λ: $\theta_{\max} = O(\Lambda^{-1})$ for $B = 0$ (solid curve).

4.2 The effect of heat losses: solution in the wafer

To describe the influence of heat transfer from the gap into the wafer material, we must obtain a representation for the temperature distribution in the wafer. We assume that $\epsilon_w \ll 1$ (i.e. the wafer is very deep compared to the gap height) and look for the leading-order solution in the wafer. Setting $\theta_w(X, 0) = \theta_0(X)$, the solution of (32) in a semi-infinite medium is [3][9]

$$\theta_w(X, \zeta) = -\frac{\zeta}{2\sqrt{\pi}} \int_0^X \frac{\theta_0(s) e^{-\zeta^2/4(X-s)}}{(X-s)^{3/2}}\, ds. \tag{35}$$

Differentiating, we find that, on $\zeta = 0$, [10]

$$\frac{\partial \theta_w}{\partial \zeta} = \frac{1}{\sqrt{\pi}} \frac{\mathrm{d}}{\mathrm{d}X} \left(\int_0^X \frac{\tau(s)}{\sqrt{X-s}}\, ds \right). \tag{36}$$

Thus, since $\theta = \theta_w$ at the interface, we find that the effective boundary condition at $Z = 0$ is

$$\frac{D\epsilon_w}{\epsilon} \frac{\partial \theta}{\partial Z} = \frac{1}{\sqrt{\pi}} \frac{\mathrm{d}}{\mathrm{d}X} \left(\int_0^X \frac{\theta(s, 0)}{\sqrt{X-s}}\, ds \right). \tag{37}$$

If the ratio D is large, $D = \mathcal{D}/\epsilon^2$, then this boundary condition will yield an additional term in (34a) which corresponds to the temperature sink generated by the presence of the conducting surface,

$$\mathrm{Pe} H \bar{U} \frac{d\theta}{dX} = \frac{d}{dX} \left(H \frac{d\theta}{dX} \right) + \mathrm{Pe}\, e^{BP} \int_0^H \left(\frac{\partial U}{\partial Z} \right)^2 dZ - \frac{1}{\sqrt{\pi \mathcal{D}}} \frac{\mathrm{d}}{\mathrm{d}X} \left(\int_0^X \frac{\theta(s, 0)}{\sqrt{X-s}}\, ds \right). \tag{38}$$

[9] This form for the solution is not immediately obvious, but the change of variables, $\mu^2 = z^2/[4(X-s)]$,

$$\theta_w = \frac{2}{\sqrt{\pi}} \int_{z/\sqrt{4X}}^{\infty} \theta_0 \left(x - \frac{z^2}{4\mu^2} \right) e^{-\mu^2}\, d\mu.$$

5 Particle effects

The abrasive particles present in the liquid slurry are typically made of copper or other metal-oxides and are harder than either the pad or the wafer surfaces. Consequently, the particles may be considered rigid and when pressed into the other surfaces, they will scratch/deform those surfaces. The key industrial questions of interest are:

- How does the presence of particles change the elasto-hydrodynamic lubrication flow?
- How do the particles affect the relation between the applied load on the asperities and the deformation δ (and the contact area scale a) and the lubrication gap scales $\bar{h}$?
- What properties of the particle slurry are most important in determining the rates of material removal and hence planarization?

These are very difficult questions involving the coupling of EHL with multi-phase flow. Only tentative steps toward these problems were made in the workshop, however we will outline the line of study that seems to have the most potential.

The problem simplifies if the influence of the particles on the fluid lubrication problem can be neglected. This is the case for slurries with very low concentrations of particles; this situation can be studied by examining problems for individual particles. The particles will only take an active role in the CMP process if they come in contact with the wafer surface and furthermore have sufficient normal force applied to them to yield removal of material from the wafer surface via abrasion. In general this will only be the case for particles trapped beneath asperity tips. Several articles have attempted studies of the contact mechanics between particles and asperity tips [16, 17, 5], i.e. under what conditions will particles in the surrounding flow be entrained into the lubrication gaps. Very large particles will not typically be able to enter the gaps of order $\bar{h}$. Meanwhile very small particles, with radius much smaller than $\bar{h}$, will enter the gap, but will not experience sufficient normal load to produce abrasion of the wafer. Particles in both of these ranges are called *inactive* and are believed to be irrelevant to CMP. Hence it is important the determine the range of particle radii for particles that can actively contribute to the CMP process,

$$R_{\min}(H, \mathbb{U}) \leq R \leq R_{\max}(H, \mathbb{U}); \tag{39}$$

this range can be expected to depend on the lubrication gap size, the flow velocity and possibly other parameters as well.

The idealized geometric description for a single active particle is a hard sphere trapped between two parallel plates. For a given particle radius and plate separation, the applied force needed can be found to be

$$N_1(R, H) = \frac{4\sqrt{2}}{3} R^{1/2} (2R - H)^{3/2}. \tag{40}$$

5.1 Statistical analysis

Obtaining mesoscopic and macroscopic results from this microscopic model for a single particle involves summing up contributions due to all of the active particles. Suppose that the population density distribution for particles in the slurry is given by a function $\phi(R)$, where $\int_0^\infty \phi(R)\, dR = 1$.

Then if the concentration of particles in the slurry is η then the expected normal load borne by particles for a single asperity is

$$N = \eta \int_{-1}^{1} \left(\int_{R_{\min}(H(X),\bar{U}(X))}^{R_{\max}(H(X),\bar{U}(X))} N_1(R, H(X)) \phi(R)\, dR \right) dX. \tag{41}$$

Another level of summation, over the distribution of asperities with different gap heights and contact areas, is then needed to determine the total normal load. Background for such calculations is given by the fundamental theoretical work by Greenwood and Williamson [8]. This approach should work well for low to moderate concentration of particles and should predict a linear increase in abrasion and wafer material removal rate with active particle density. For very dense slurries the removal rate can be expected to be limited by the asperity contact area (a) rather than the particle concentration (η). Some articles have addressed questions on what determines the material removal rate and how it can be modeled based on the abrasive action of the active slurry particles [1, 12, 20, 21].

A Estimated parameter values

Some reasonable values for CMP parameters, taken from [12, 13] and other sources:

- Polishing speed ($\mathbb{U}$): 150 RPM ($\approx$ 84 m/s linear speed)
- Normal load per unit area: 45 kPa
- Average asperity radius (R): 40μm
- Average asperity density per unit area: 400 asperities/mm^2
- Average asperity size (D): 5μm
- Typical slurry particle size range (R): 0.2–2.0μm
- Concentration of slurry particles (η): 5%
- Peclet number (Pe): 1–10
- Gap aspect ratio (ϵ): 0.03
- Relative length scale for the wafer (ϵ_w): 0.44
- Bearing number (Λ): 0.07
- Temperature scaling (ΔT): 0.06

References

[1] G. Ahmadi and X. Xia. A model for mechanical wear and abrasive particle adhesion during the chemical mechanical polishing process. *Journal of the electrochemical society*, 148(3):G99–109, 2001.

[2] A. Cameron. *Basic Lubrication Theory, third edition*. John Wiley, New York, 1981.

[3] H. S. Carslaw and J. C. Jaeger. *Conduction of heat in solids, 2nd ed.* Oxford University Press, New York, 1959.

[4] M. S. Carvalho and L. E. Scriven. Deformable roll coating flows: steady state and linear perturbation analysis. *Journal of Fluid Mechanics*, 339:143–172, 1997.

[5] F. Chinas-Castillo and H. A. Spikes. Mechanism of action of colloidal solid dispersions. *Journal of Tribology: Transactions of the ASME*, 125:552–557, 2003.

[6] D. Dowson and G. R. Higginson. *Elastohydrodynamic lubrication*. Pergamon Press, 1977.

[7] M. J. Gostling, M. D. Savage, A. E. Young, and P. H. Gaskell. A model for deformable roll coating with negative gaps and incompressible compliant layers. *Journal of Fluid Mechanics*, 489:155–184, 2003.

[8] J. A. Greenwood and J. B. P. Williamson. Contact of nominally flat surfaces. *Proceedings of the Royal Society of London A*, 295(1442):300–319, 1966.

[9] B. J. Hamrock. *Fundamentals of fluid film lubrication*. McGraw-Hill, New York, 1994.

[10] P. D. Howell and C. J. W. Breward. Mathematical modelling of the overflowing cylinder experiment. *Journal of Fluid Mechanics*, 474:275–298, 2003.

[11] S. Howison. *Practical applied mathematics*. Cambridge University Press, New York, 2005.

[12] Y.-R. Jeng and P.-Y. Huang. Impact of abrasive particles on the material removal rate in CMP. *Electrochemical and solid-state letters*, 7(2):G40–43, 2004.

[13] Y.-R. Jeng and H.-J. Tsai. Improved model of wafer/pad powder slurry for cmp. *Journal of the Electrochemical society*, 150(6):G348–354, 2003.

[14] O. E. Jensen and J. B. Grotberg. The spreading of heat or soluble surfactant along a thin liquid film. *Physics of Fluids A*, 5(1):58–68, 1993.

[15] K. L. Johnson. *Contact mechanics*. Cambridge University Press, New York, 1985.

[16] G. K. Nikas. Mathematical analysis of the entrapment of solid spherical particles in non-conformal contacts. *Journal of Tribology: Transactions of the ASME*, 123:83–93, 2001.

[17] G. K. Nikas. Particle entrainment in elastohydrodynamic point contacts and related risks of oil starvation and surface indentation. *Journal of Tribology: Transactions of the ASME*, 124:461–467, 2002.

[18] A. Z. Szeri. *Fluid film lubrication*. Cambridge University Press, New York, 1998.

[19] D. G. Takurta, C. L. Borst, D. W. Schwendeman, R. J. Gutmann, and W. N. Gill. Pad porosity, compressibility and slurry delivery effects in chemical-mechanical planarization: modeling and experiments. *Thin solid films*, 366:181–190, 2000.

[20] D. Tamboli, G. Banerjee, and M. Waddell. Novel interpretations of CMP removal rate dependencies on slurry particle size and concentration. *Electrochemical and solid-state letters*, 7(10):F62–65, 2004.

[21] D. G. Thakurta, D. W. Schwendeman, R. J. Gutmann, S. Shankar, L. Jiang, and W. N. Gill. Three-dimensional wafer-scale copper chemical-mechanical planarization model. *Thin solid films*, 414:78–90, 2002.